



Fast Track

Comparative Transcriptomic Analysis of MAPK-Mediated Regulation of Sectorization in *Cryphonectria parasitica*

Jeesun Chun¹, Kum-Kang So¹, Yo-Han Ko², Jung-Mi Kim³, and Dae-Hyuk Kim^{1,2,4,*}

¹Institute for Molecular Biology and Genetics, ²Department of Bioactive Material Sciences, Chonbuk National University, Chonbuk 54896, Korea, ³Department of Bio-Environmental Chemistry, Institute of Life Science and Natural Resources, Wonkwang University, Chonbuk 54538, Korea, ⁴Department of Molecular Biology, Chonbuk National University, Chonbuk 54896, Korea

*Correspondence: dhkim@jbnu.ac.kr
<http://dx.doi.org/10.14348/molcells.2019.0019>
www.molcells.org

Fungal sectorization is a complex trait that is still not fully understood. The unique phenotypic changes in sporadic sectorization in mutants of *CpBck1*, a mitogen-activated protein kinase kinase kinase (MAPKKK) gene, and *CpSit2*, a mitogen-activated protein kinase (MAPK) gene, in the cell wall integrity pathway of the chestnut blight fungus *Cryphonectria parasitica* have been previously studied. Although several environmental and physiological factors cause this sectoring phenotype, genetic variants can also impact this complex morphogenesis. Therefore, RNA sequencing analysis was employed to identify candidate genes associated with sectorization traits and understand the genetic mechanism of this phenotype. Transcriptomic analysis of *CpBck1* and *CpSit2* mutants and their sectorized progeny strains revealed a number of differentially expressed genes (DEGs) related to various cellular processes. Approximately 70% of DEGs were common between the wild-type and each of *CpBck1* and *CpSit2* mutants, indicating that *CpBck1* and *CpSit2* are components of the same MAPK pathway, but each component governs specific sets of genes. Functional description of the DEGs between the parental mutants and their sectorized progenies revealed several key pathways, including the biosynthesis of secondary metabolites, translation, amino acid metabolism, and carbohydrate metabolism; among these, pathways for secondary

metabolism and translation appeared to be the most common pathway. The results of this comparative study provide a better understanding of the genetic regulation of sector formation and suggest that complex several regulatory pathways result in interplays between secondary metabolites and morphogenesis.

Keywords: MAPK pathway, RNA-Seq, sectorization, transcriptomic analysis

INTRODUCTION

Filamentous fungal sectorization, which is called ‘woolly degeneration’ and was first reported in the model organism *Neurospora crassa* (Sheng, 1951), occurs during subculture on artificial media showing loss or reduced asexual sporulation, fruiting, and sexual propagation (Ryan et al., 2002; Wang et al., 2004). These degenerative morphological states are accompanied by a decrease in secondary metabolite production, causing substantial commercial losses (Li et al., 1994; Magae et al., 2005). However, the underlying mechanism of colony sectorization is not fully understood.

Received 12 February, 2019; accepted 21 February, 2019; published online 4 April, 2019

eISSN: 0219-1032

© The Korean Society for Molecular and Cellular Biology. All rights reserved.

© This is an open-access article distributed under the terms of the Creative Commons Attribution-NonCommercial-ShareAlike 3.0 Unported License. To view a copy of this license, visit <http://creativecommons.org/licenses/by-nc-sa/3.0/>.

In *Cryphonectria parasitica*, mitogen-activated protein (MAP) kinases is a great concern because several components in MAPK pathways and their downstream effectors are modulated by the presence of the single-stranded RNA Cryphonectria Hypovirus 1 (CHV1) or are involved in hypoviral symptom development, such as reduced pathogenicity and hydrophobicity (Choi et al., 2005; Deng et al., 2007; Kim et al., 2010; Park et al., 2004; 2012; So and Kim, 2017; Sun et al., 2009; Turina et al., 2006). Among these MAPK pathways, the cell wall integrity (CWI) MAPK pathway is unique because a mutant of *CpBck1*, an ortholog of yeast Bck1 (a CWI MAPKKK), and *CpSlt2*, an ortholog of yeast Slt2 (a CWI MAPK), have shown characteristic phenotypic changes of sporadic sectorization. Moreover, when the sectorized mycelia of each mutant strain were successively transferred to new media, the progenies of the sectorized mutant maintained sectorized phenotypes, indicating that, once sectorized, the sectorized phenotype was stably inherited. In addition, we found that the sectorized progenies of *CpBck1* and *CpSlt2* had drastic impaired virulence, although they had partially retrieved the mycelial growth (Kim et al., 2016; So et al., 2017). A recent study on the underlying genetic mechanism governing these sectorized phenotypes identified global epigenetic changes in sectorized progenies (So et al., 2018). However, further studies are required to understand both the genes affected in sectorized progenies and their regulation.

Massive transcripts analyses are useful to obtain comprehensive information on the regulation of genes involved in stable phenotypic changes such as sectorization. Differential mRNA display (Chen et al., 1996; Kang et al., 2000) and cDNA microarray representing approximately 2,200 unique genes (Allen et al., 2003) were conducted in *C. parasitica* to determine the genes affected by hypovirus infection or mutations in one or more key regulatory pathways. However, differential mRNA display requires considerable additional efforts to determine the identity of differentially expressed genes (DEGs) and microarray can provide information only on given sequences. In contrast, using high-throughput sequencing, genome-wide transcript profiling is possible by directly sequencing the mRNAs in a sample. Therefore, RNA sequencing technology (RNA-Seq) is considered to be the most powerful tool for transcriptomic analysis. In this study, we conducted transcriptomic analysis using RNA-Seq and compared transcript profiles between the mutant strains and the wild-type. Further comparison was performed between the sectorized progenies of the mutant strains and their corresponding parental strains to obtain comprehensive information on the genes involved in sectorization to identify the specific genes underlying sectorization.

MATERIALS AND METHODS

Fungal strains and paired-end RNA sequencing

C. parasitica wild-type strain EP155/2 (ATCC 38755) its isogenic hypovirus-CHV1-713-containing strain UEP1, the CWI MAPKKK deletion mutant TdBCK1 and its sectorized progeny TdBCK1-S1, and the CWI MAPK deletion mutant TdSLT2-69 and its sectorized progeny TdSLT2-69-S1 were used for the

RNA-Seq analysis. The strains were grown on PDAMB under standard growth conditions at 25°C under low constant light. For the RNA-Seq analysis, 5-day-old mycelia were harvested from the cellophane membrane. Total RNA was extracted as described previously (Kim et al., 1995). The cDNA libraries for three biological repeats for each sample were sequenced using the Illumina HiSeq 2000 system, producing 47.5 Gbp of 101-bp paired-end reads. The extracted sequences were trimmed at a phred score of 20 and kept paired reads with a length of 25-bp using SolexaQA (Langmead et al., 2009). Qualified clean reads were mapped on annotated gene transcripts of the reference *C. parasitica* genome (<http://genome.jgi-psf.org/Crypa2/Crypa2.home.html>) using Bowtie 2 (v2.1.0) software (Chae et al., 2017; Li et al., 2010; Moon et al., 2018). Read counts were normalized by DESeq library (Anders and Huber, 2010) implemented in software R package.

RNA-Seq data analysis

The differentially expressed value of the assembled unique transcripts was calculated and normalized using the Fragments Per Kilobase of exon per Million (FPKM) method by dividing the number of fragments mapped to each gene by the size of its transcripts. False Discovery Rate (FDR), obtained by converting the statistical score to p -value using binomial distribution, was used to rule out any possibility of false positive and identify the threshold p -value. Genes with p -value less than 0.01 were regarded as significantly expressed. Fold Change (FC) analyses were performed to identify differentially expressed genes (DEGs) between each samples. DEG were identified by twofold change in reads for all pairwise comparisons based on the FPKM counts. To assess the differential transcript level between pairwise comparisons, a threshold of \log_2 -fold change larger than 1 and smaller than -1 in expression were taken into consideration as significantly up- or down-regulated in this study, respectively. For functional annotation of the DEGs, the assembled unique transcripts were compared with the amino acid sequences using the BLASTX analysis against the non-redundant database with cutoff E -value of $1e-10$. The DEGs were annotated to generate Gene Ontology (GO) terms according to biological process, cellular component and molecular function (counts ≥ 1). In addition, biochemical and metabolic pathway of the DEGs were analyzed according to Kyoto Encyclopedia of Genes and Genomes (KEGG) pathway database of the reference strain *Magnaporthe oryzae*.

Validation of DEGs by qRT-PCR analysis

To validate the DEGs, qRT-PCR analysis was conducted for 18 selected DEGs, selected based on the significant fold changes caused by the presence of hypovirus as well as sectorization. RNA was extracted from all tested strains cultured for five days on PDAMB plates, and first-strand cDNA was synthesized from 500 ng of RNA using SuperScript III reverse transcriptase (Invitrogen Corp., USA) with random primers. Real-time PCR was performed using an Applied Biosystems 7500 system with SYBR premix Ex Taq II (TaKaRa, Japan). Analyses were conducted in triplicate for each transcript as

technical replicates, and at least two biological replications were performed using independent RNA preparations of the tested sample. Transcript levels were normalized to the mRNA values of the internal control gene of glyceraldehyde-3-phosphate dehydrogenase (GenBank No. P19089), and the relative gene expression level was analyzed with the $2^{-\Delta\Delta CT}$ method (Livak and Schmittgen, 2001). Table 4 lists the genes used for the qRT-PCR analysis. The correlation between two platforms were analyzed by linear regression analysis and statistical significance of the regression coefficient was determined by *t*-test.

Statistical analysis

All quantitative real-time RT-PCR transcripts were analyzed with analysis of variance using SPSS software (ver. 23.0, SPSS Inc., USA). The significance of all effects was determined using the Student-Newman-Keuls method at a significance level of $p = 0.01$.

RESULTS AND DISCUSSION

Overview of RNA-Seq

To characterize the MAPK-mediated transcriptional regulation of sectorization, RNA-Seq analyses were performed on the mutant strain of TdBCK1 referring a transformant deleted the *CpBck1* gene, an ortholog of yeast CWI MAPKKK, and on TdSLT2-69 referring a transformant deleted the *CpSl2* gene, an ortholog of yeast CWI MAPK, in comparison with the wild-type EP155/2 strain. In addition, the corresponding sectorized progenies of TdBCK1 and TdSLT2-69, TdBCK1-S1 and TdSLT2-69-S1, were included to obtain information on sector-specific genome-wide transcriptional

changes. RNA samples were isolated after 5 days of cultivation on potato dextrose agar medium supplemented with methionine and biotin (PDAMB), cDNA libraries for three biological replicates for each sample were prepared, and 15 datasets were sequenced using Illumina HiSeq 2000 platform. More than 2.85×10^8 qualified 101-bp paired-end reads were generated, and approximately 62.3% of short reads were successfully mapped either uniquely or multiply on annotated gene transcripts of the reference *C. parasitica* genome (<http://genome.jgi-psf.org/Crypa2/Crypa2.home.html>). The unmapped reads might be derived from mapping errors in spite of quality filtration or an incomplete annotation of the reference genome. However, the unmapped reads in this study appeared lower than those reported by others ranging from 46.2% to 47.6% (Cox et al., 2010).

Using a \log_2 -fold change (FC) cutoff, DEGs were identified from a pair-wise comparison (Fig. 1). In total, 458 and 433 unique transcripts of TdBCK1 and TdSLT2-69, respectively, were identified as DEGs compared to the wild-type (Supplementary Table S1). Of these, 224 genes were up-regulated, and 234 were down-regulated in TdBCK1, whereas 224 genes were up-regulated, and 209 were down-regulated in TdSLT2-69. Interestingly, 321 genes were common DEGs in the TdBCK1 and TdSLT2-69 mutants, which represented 70% and 74% of the DEGs in each mutant strain, respectively. The high proportion of common DEGs indicated that the *CpBck1* and *CpSl2* genes were in the same regulatory pathway, confirming that *CpBck1* is a MAPKKK and *CpSl2* is a MAPK in the same CWI MAPK signaling pathway. Moreover, approximately 30% of DEGs were identified as independently regulated, suggesting that the existence of component-specific regulatory pathways.

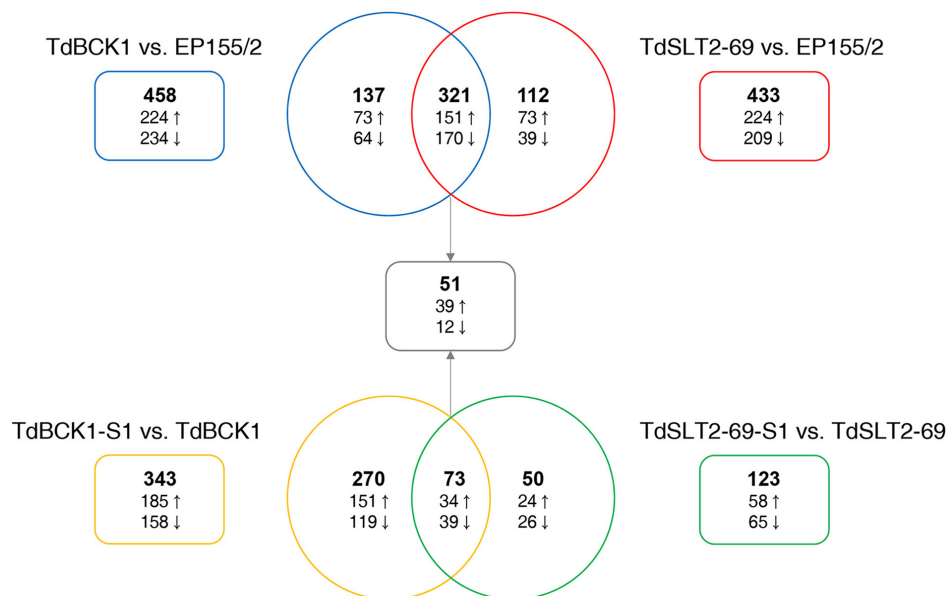


Fig. 1. Venn diagram of DEGs in a pair-wise comparison of the strains. The DEGs are represented between the strains compared, and the arrows indicate up- and down-regulation. The 51 overlapping DEGs caused by the *CpBck1* and *CpSl2* mutations as well as sectorization are indicated at the ends of the arrows from the two Venn diagrams.

Table 1. DEGs with $|\log_2(\text{fold change})| > 4$ in TdBCK1-S1 compared to TdBCK1 and TdSLT2-69-S1 compared to TdSLT2-69, respectively

JGI gene ID	Log ₂ (FC): TdBCK1-S1 vs. TdBCK1	Function description
245902	9.59	Cytochrome P450
35639	8.52	Cytochrome P450
324947	8.31	Hypothetical protein
248498	8.02	Trichothecene 3-O-acetyltransferase
32824	7.67	AndM
283813	6.37	Hypothetical protein
245011	6.37	Polyketide synthase
338852	6.32	Polyketide synthase 4
323706	6.13	
258342	5.60	Putative sodium phosphate protein
85578	5.49	
346810	5.47	Putative nacht domain protein
100383	5.39	Cryparin
278307	5.13	Putative 3-amino-3-carboxypropyl transferase
356022	4.62	Putative acid phosphatase
39663	4.41	Putative mfs multidrug protein
287230	4.20	Putative major facilitator superfamily transporter phosphate
79318	4.18	Putative 3-phytase a
336241	-4.28	Putative calcium-translocating p-type atpase
323670	-4.43	Specific serine endopeptidase
354483	-4.64	LysM domain protein, putative
86125	-5.56	Acyl transferase/acyl hydrolase/lysophospholipase
13424	-7.22	Putative TPA
343514	-9.83	Putative aristolochene synthase protein

JGI gene ID	Log ₂ (FC): TdSLT2-69-S1 vs. TdSLT2-69	Function description
85578	10.19	
258342	4.77	Putative sodium phosphate protein

Transcriptomic analysis of the sectorized strain of the *CpBck1*-null mutant (TdBCK1-S1) compared to that of the parental *CpBck1*-null mutant strain (TdBCK1) revealed that a total of 343 genes were differentially expressed; 185 genes of these were up-regulated, and 158 were down-regulated. Comparing TdSLT2-69 and TdSLT2-69-S1, a total of 123 genes were differentially regulated; 58 of these genes were up-regulated, and 65 were down-regulated. Table 1 presents the highly expressed transcripts for each strain showing $|\log_2(\text{fold change})| > 4$. There were similar number of DEGs (i.e., 458 and 433) between the mutants and the wild-type (TdBCK1 vs. EP155/2 and TdSLT2-69 vs. EP155/2), but there was a 2.8-fold difference in DEGs (i.e., 343 and 123) between the sectorized progenies and the corresponding parental mutant strains (TdBCK1-S1 vs. TdBCK1 and TdSLT2-69-S1 vs. TdSLT2-69). Considering the severe phenotypic changes in the *CpBck1* mutant lines compared to those of *CpSlt2* mutant lines, the larger number of DEGs between TdBCK1 and TdBCK1-S1 is consistent with the degree of phenotypic changes. Accordingly, a large number of DEGs between TdBCK1 and TdBCK1-S1 might be involved in processes other than sectorization, and the DEGs between

TdSLT2-69 and TdSLT2-69-S1 were more specific to sectorization.

Among the 466 genes that were differentially expressed based on the two comparisons (TdBCK1-S1 vs. TdBCK1 and TdSLT2-69-S1 vs. TdSLT2-69), 73 genes were identified as common DEGs affected in both comparisons (TdBCK1-S1 vs. TdBCK1 and TdSLT2-69-S1 vs. TdSLT2-69), showing transcriptional alteration in the same direction in both comparisons. Of these 73 genes, 34 were up-regulated, and 39 were down-regulated compared with the parental mutants and their corresponding sectorized progenies. Moreover, 59 of the 73 genes were affected in the comparison between the wild-type and the parental mutant TdBCK1, and 51 of the 73 genes were differentially expressed between the wild-type and the parental mutant TdSLT2-69. All 51 DEGs were differentially expressed between the wild-type and TdBCK1. Therefore, 51 DEGs were affected by mutation and further affected by sectorization. Interestingly, 22 of the 73 genes were affected by the presence of CHV1, indicating a significantly overlapped difference in transcription between EP155/2 and UEP1 (data not shown). However, the transcriptional changes of these 22 DEGs were not altered in the

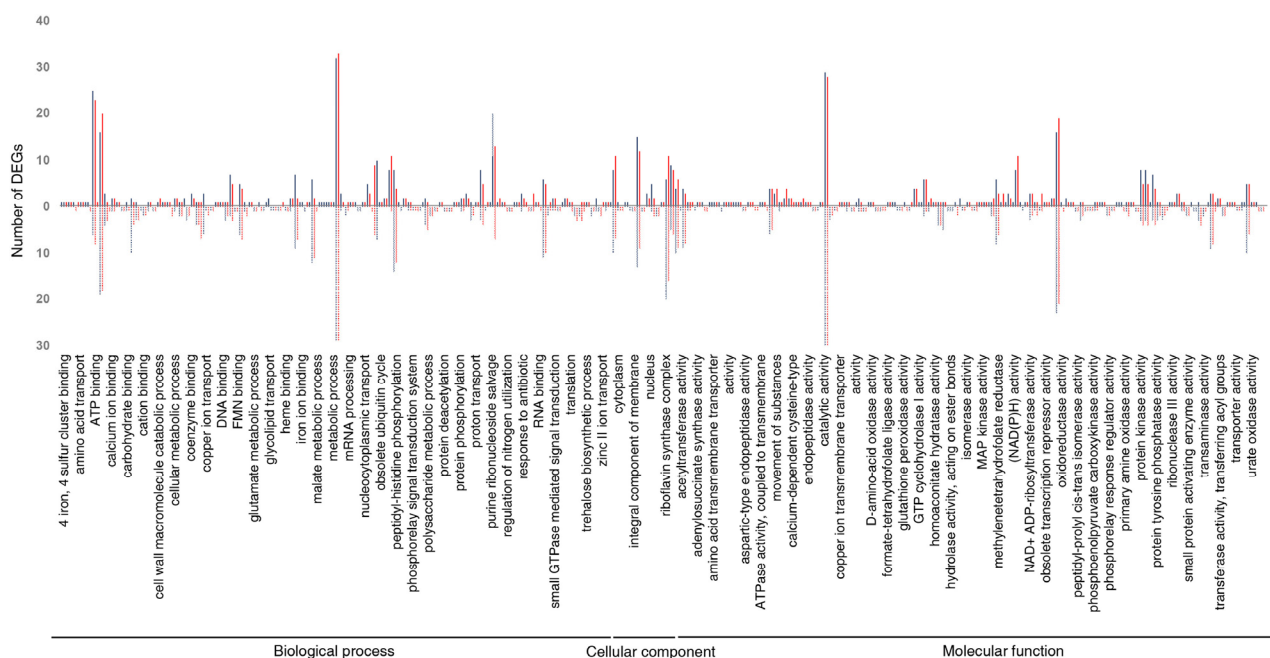


Fig. 2. GO analysis of up- and down-regulated DEGs in TdBCK1 (blue) and TdSLT2-69 (red) compared to the wild-type. All DEGs were further classified into biological process, cellular component, and molecular function sub-categories. The filled bars represent the up-regulated DEGs, and the dashed bars represent the down-regulated DEGs.

same direction i.e., 14 viral up-regulated genes were divided into 8 up-regulated and 6 down-regulated, whereas 8 viral down-regulated genes were divided into 7 up-regulated and 1 down-regulated in sectorization comparisons.

Functional analysis of DEGs

GO analysis was performed for the up-regulated genes in TdBCK1 compared to the wild-type (Fig. 2). GO analysis revealed enrichment in the biological process and molecular function categories. Metabolic process was the dominant enriched biological process category, followed by the ATP binding, binding, zinc ion binding, proteolysis, and nucleic acid binding categories, with at least 10 up-regulated genes. In the cellular component ontology, intracellular, integral component of membrane, membrane, and nucleus were four dominant enriched categories, with at least 13 DEGs. Catalytic activity and oxidoreductase activity were the two most strongly influenced ontologies in the molecular function category. Down-regulated genes showed similar enrichment of the biological process category as up-regulated genes, except that the number of down-regulated genes in the ATP binding category was markedly reduced compared to that of up-regulated genes. Integral component of membrane, membrane, and nucleus were the top three enriched cellular component categories, with more than nine DEGs. Catalytic activity and oxidoreductase activity were again the top two enriched categories in molecular function, followed by transporter activity, transcription factor activity, and monooxygenase activity. Interestingly, the biological process

included categories showing a large difference between up-regulated and down-regulated genes. For example, a more than two-fold increase in down-regulated DEGs was observed in iron ion binding and carbohydrate metabolic process categories when categories with more than 10 DEGs were included.

GO analysis was performed in TdSLT2-69 compared to the wild-type (Fig. 2). GO analysis revealed enrichment in the biological process and molecular function categories. In the biological process categories, zinc II ion transport and gluconeogenesis were the top two most enriched categories in terms of both up- and down-regulated genes; this was followed by cellular metabolic process, cation transport, and sequence specific DNA binding. Most DEGs in the cation transport category were up-regulated, whereas other enriched categories showed similar numbers of up- and down-regulated genes. In the cellular component ontology, ribosome and intracellular were the first and second most influenced categories, respectively, and intracellular was also an enriched category in TdBCK1. In the molecular function category, ATPase activity, coupled to the transmembrane movement of substances, was the dominant enriched category, followed by urate oxidase activity, methionine adenosyltransferase activity, transferase activity, amidophosphoribosyltransferase activity, oxidoreductase activity, adenosylhomocysteinase activity, adenosine kinase activity, and protein tyrosine/serine/threonine phosphatase activity. Among these enriched categories, adenosylhomocysteinase activity and adenosine kinase activity were enriched with mostly up-

regulated genes, whereas amidophosphoribosyltransferase activity, oxidoreductase activity, and protein tyrosine/serine/threonine phosphatase activity were enriched with more down-regulated genes.

Considering that a large proportion of DEGs were commonly obtained, common categories of ontology were expected. In total, 179 common categories of the 270 and 230 categories obtained in the comparisons of TdBCK1 vs. EP155/2 and TdSLT2-69 vs. EP155/2, respectively were identified. In addition, the enriched pattern of categories were maintained in common categories i.e., dominant categories for each comparison remained dominant in common categories. However, there were unique categories in each comparison. These results suggest that, although there are significant overlaps in terms of downstream target genes, component-specific pathways exist, and the effects of the component on each target gene differ significantly in the CWI MAPK pathway. GO analysis of common categories indicated that *CpBck1* and *CpSl2*, components of the well-known CWI MAPK pathway, have multiple roles in governing the cell development process via diverse metabolisms related to amino acid, carbohydrate, secondary metabolites, and transport. These broad spectrums of GO enrichment are consistent with the fact that the fungal cell wall is composed primarily of chitin, glucans, other polysaccharides, and glycoproteins and cell wall formation involves numerous biosynthetic pathways of hundreds of gene products (Bowman and Free, 2006). In addition, the enriched common cellular components included the membrane, which is known to harbor many cell wall-synthesizing enzymes for the primary cell wall components that form extracellular cross-linkage. Therefore, we examined the expression profiles of repre-

sentative cell wall synthesizing enzymes (Fig. 3). Chitin, a linear homopolymer of β -1,4-linked *N*-acetylglucosamine, synthesized by chitin synthase, is an important cell wall component for cell wall integrity. Four and three putative chitin synthases were differentially expressed in TdBCK1 and TdSLT2-69 compared to the wild-type, respectively (Fig. 3A). These chitin synthases were similarly regulated, showing similar up- and down-regulation i.e., two down-regulated DEGs of TdSLT2-69 were also down-regulated in TdBCK1 and one up-regulated DEG was up-regulated in TdBCK1 as well. Thus, only one DEG was specific to TdBCK1, suggesting that *CpBck1* and *CpSl2* were in the same regulatory pathway, although there also appeared to be a component-specific downstream effect. In addition, not all chitin synthases were regulated by the CWI MAPK pathway, because the genome database survey indicated that there were nine putative chitin synthases, of which only four were specifically affected by the CWI MAPK component mutations. Similarly, 18 of 21 glycoside hydrolases, which were assumed to be involved in the cross-linking of cell wall components, were differentially regulated in TdBCK1; most of these were down-regulated, and only two were up-regulated. Nine genes were affected in TdSLT2-69, all of which were also affected in TdBCK1 in the same regulatory direction.

GO analysis was performed in TdBCK1-S1 compared to its parental TdBCK1 strain (Fig. 4), revealing enrichment of the biological process and molecular function categories. In the biological process categories, metabolic process was the dominant category, followed by binding, ATP-binding, transport, zinc ion binding, and proteolysis, with more than 15 DEGs. The top two categories in the cellular component ontology were integral component of membrane and

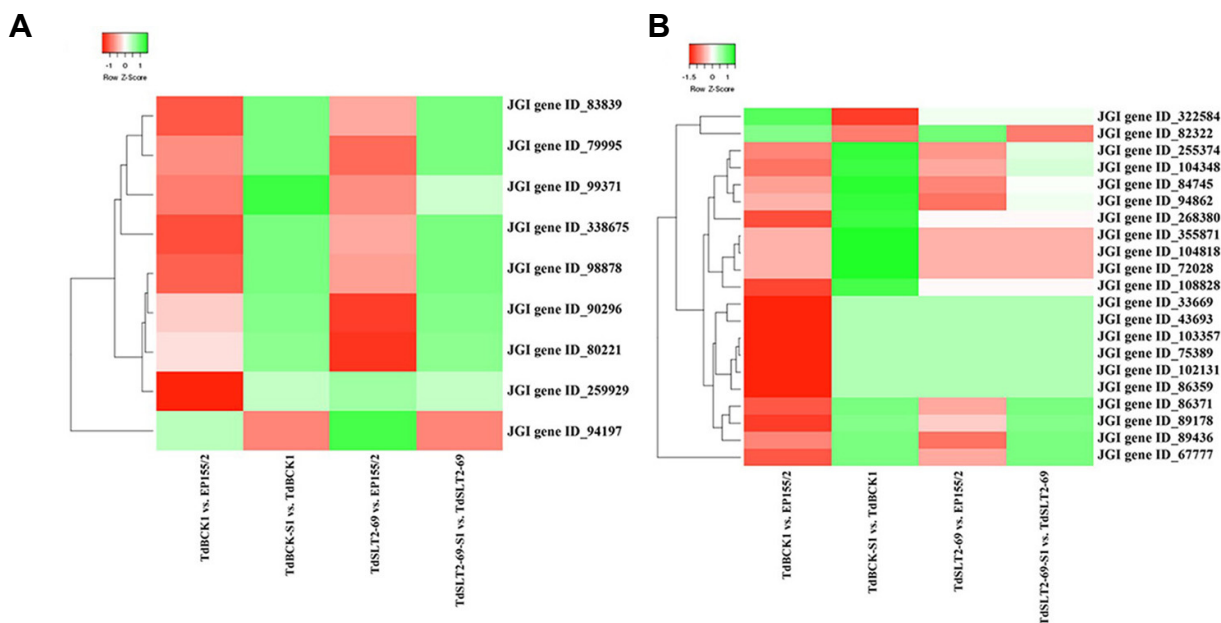


Fig. 3. Heat maps showing up- and down-regulated (A) chitin synthase and (B) glycoside hydrolase involved in fungal cell wall formation. Green shading represents up-regulated expression, and red shading represents down-regulated expression. Strains (column) and genes (row) are hierarchically clustered based on Pearson's correlation.

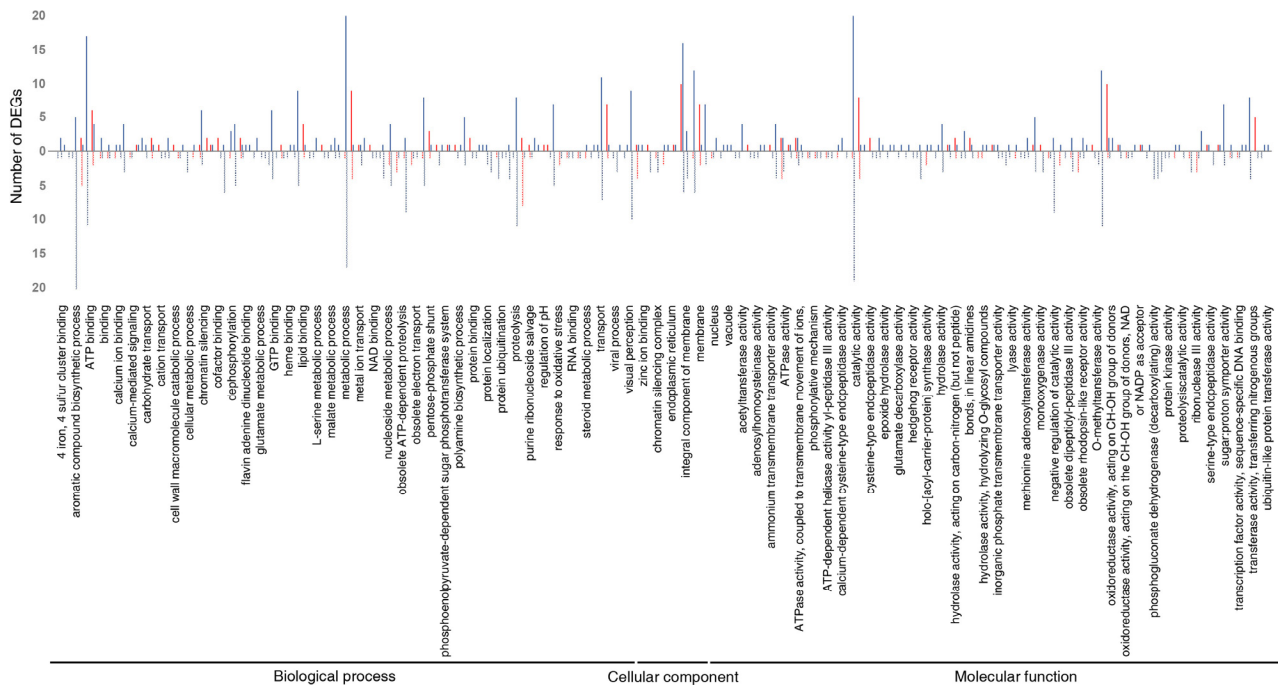


Fig. 4. GO analysis of up- and down-regulated DEGs in TdBCK1-S1 (blue) and TdSLT2-69-S1 (red) compared to their respective parental strains. All DEGs were further classified into biological process, cellular component, and molecular function sub-categories. The filled bars represent the up-regulated DEGs, and the dashed bars represent the down-regulated DEGs.

membrane. In addition, catalytic activity and oxidoreductase activity were the top categories in molecular function. GO analysis of the comparison between TdSLT2-69 and TdSLT2-69-S1 revealed enrichment of the biological process and molecular function categories. Metabolic process, proteolysis, transport, and binding were the top four categories in the biological process ontology. Although the dominant categories of the TdSLT2-69-S1 comparison were similar to those of the TdBCK1-S1 comparison i.e., integral component of membrane and membrane were the top two categories in the cellular component and catalytic activity and oxidoreductase activity were the top two categories in the molecular function categories, respectively, there were specific enriched categories for each comparison.

More GO categories per DEG were detected from the comparisons of the sectorized progeny and their corresponding parental strains than between the mutant strains and the wild-type. This suggested that sectorization affected a broader and different spectrum of genes. Among the three chitin synthases affected in the mutants from the wild-type, only one chitin synthase gene was differentially regulated in TdBCK1-S1 but not in TdSLT2-69-S1, and the direction of alteration differed (Fig. 3A). Likewise, among the 18 glycoside hydrolase DEGs in TdBCK1, 8 were affected, all of which showed opposing regulatory directions (Fig. 3B). More interestingly, three new glycoside hydrolases were up-regulated in TdBCK1-S1 (Fig. 3B). Of the nine affected DEGs in TdSLT2-69, only one was differentially expressed in TdSLT2-69-S1 with the opposite regulatory direction, which was the only one differentially regulated in both comparisons i.e., down-

regulated in both mutants from the wild-type and up-regulated in the sectorized progenies from the parental mutant strains. Considering that phenotypic changes occurred to a lesser extent in TdSLT2-69 than in TdBCK1, it was expected that more DEGs of cell wall-synthesizing enzymes would be identified in the comparison of TdBCK1. In addition, robust mycelial growth in the sectorized progenies was evidenced by the opposite direction of the transcriptional alteration of the sectorized progenies compared to the parental mutant strains. However, only one DEG encoding a putative glycoside hydrolase family 16 protein was common in all comparisons, i.e., up-regulated in the TdBCK1 and TdSLT2-69 mutants vs. the wild-type and down-regulated in the TdBCK1-S1 and TdSLT2-69-S1 vs. the parental mutants. These results suggest that a sectorization-specific, rather than a cell wall integrity-specific, transcriptional regulatory mechanism exists and common DEGs of the comparisons between TdBCK1-S1 vs. TdBCK1 and TdSLT2-69-S1 vs. TdSLT2-69 are likely to play important roles in sectorization. Thus, GO analysis was performed for the 73 common DEGs, affected in both TdBCK1-S1 vs. TdBCK1 and TdSLT2-69-S1 vs. TdSLT2-69 (Fig. 5). Proteolysis, metabolic process, and ATP-binding were the top three categories in the biological process ontology. Membrane and integral component of membrane were the two dominant cellular component categories. Aspartic-type endopeptidase activity, catalytic activity, and oxidoreductase activity were the top three assign terms in the molecular function. These results suggest that sectorization is a complex trait involving a broad spectrum of target genes that affect fungal physiology, membrane function, and redox potential.

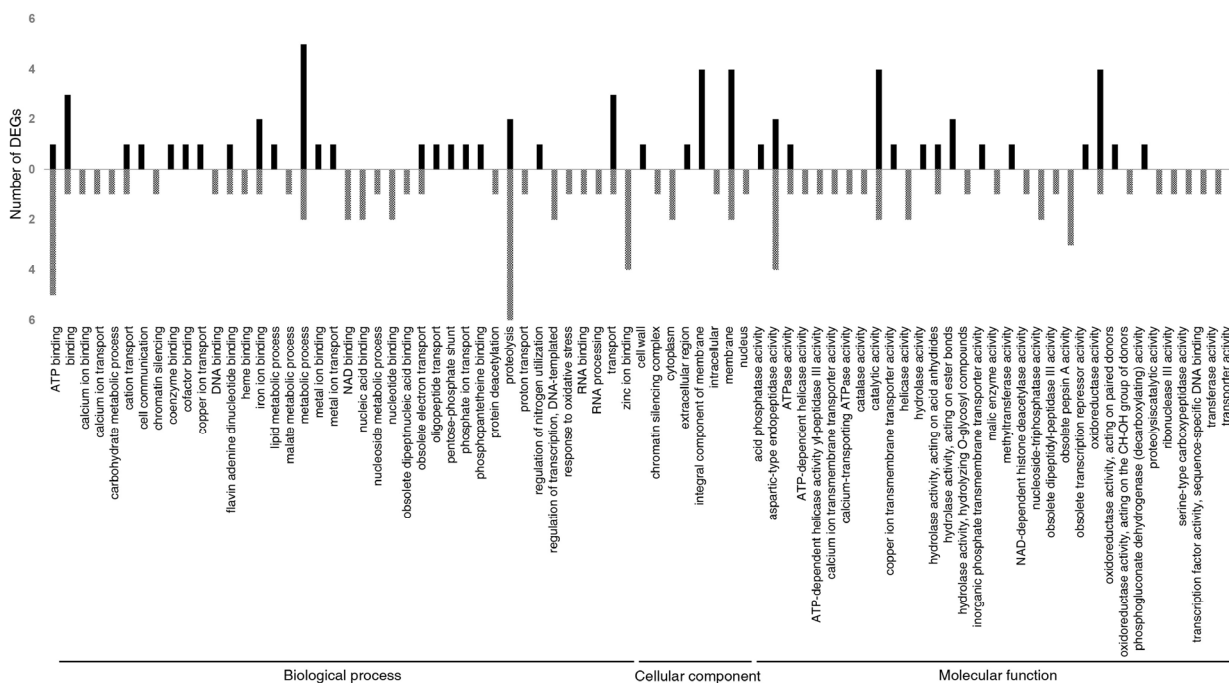


Fig. 5. GO analysis of up- and down-regulated common DEGs in TdBCK1-S1 and TdSLT2-69-S1 compared to their parental strains. All DEGs were further classified into biological process, cellular component, and molecular function sub-categories. The black-filled bars represent the up-regulated DEGs, and the gray-filled bars represent the down-regulated DEGs.

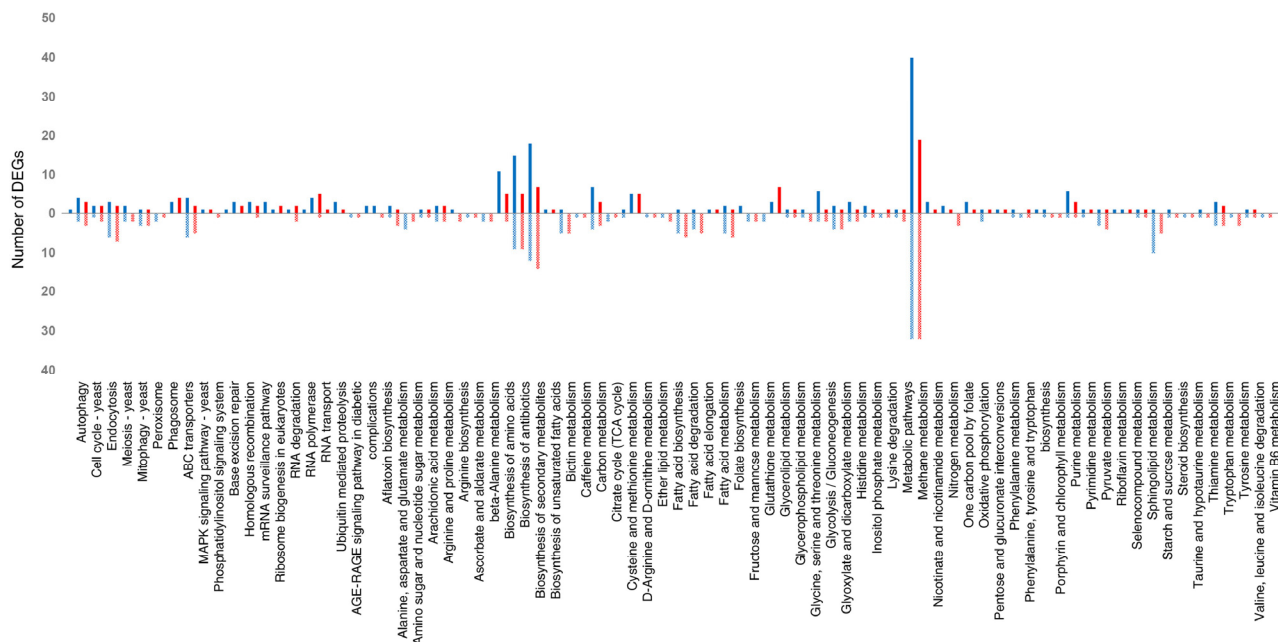


Fig. 6. KEGG pathway analysis of DEGs in TdBCK1 (blue) and TdSLT2-69 (red) compared to the wild type. The filled bars represent the up-regulated DEGs, and the dashed bars represent the down-regulated DEGs.

Additionally, DEGs were subjected to KEGG pathway analysis. Biosynthesis of other secondary metabolites was the most prominent pathway in the TdBCK1 mutant (Fig. 6).

Moreover, amino acid metabolism, carbohydrate metabolism, and lipid metabolism pathways were significantly represented. Signal transduction pathways, including the MAPK

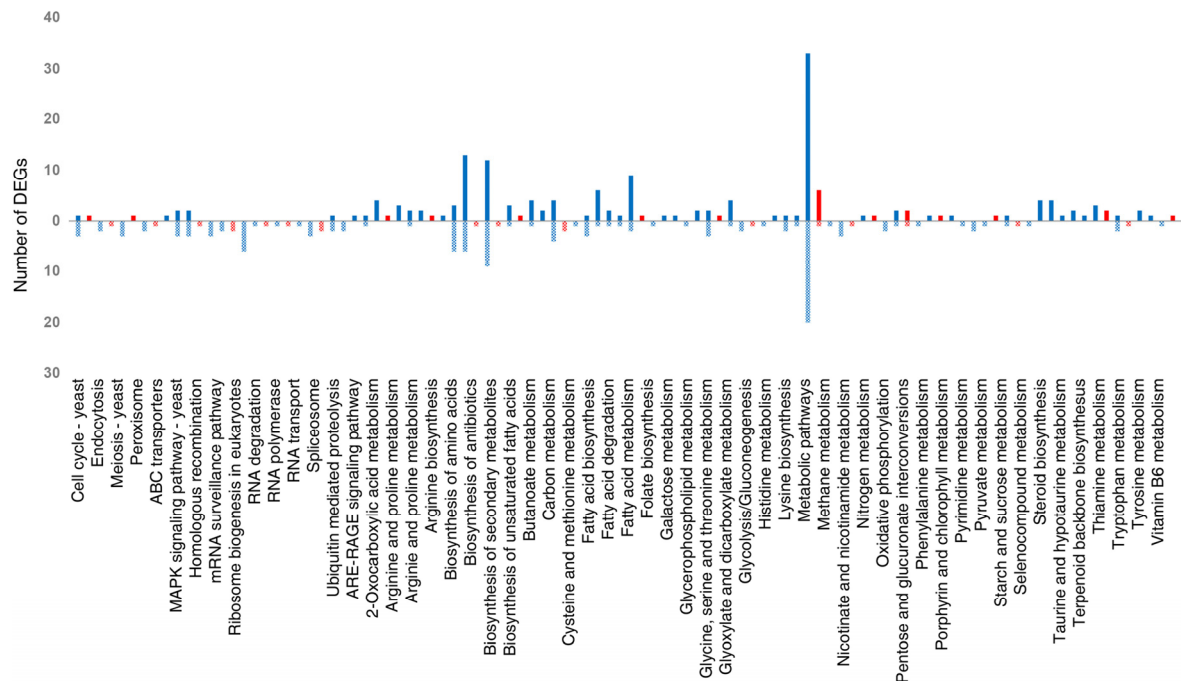


Fig. 7. KEGG pathway analysis of DEGs in TdBCK1-S1 (blue) and TdSLT2-69-S1 (red) compared to their parental strains. The filled bars represent the up-regulated DEGs, and the dashed bars represent the down-regulated DEGs.

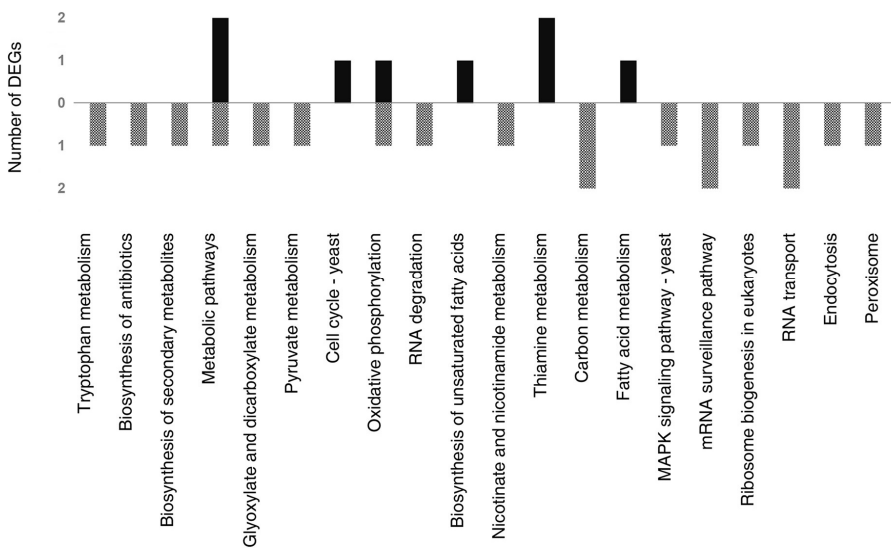


Fig. 8. KEGG pathway analysis of common DEGs in TdBCK1-S1 and TdSLT2-69-S1 compared to their parental strains. The black-filled bars represent the up-regulated DEGs, and the gray-filled bars represent the down-regulated DEGs.

signaling pathway and phosphatidylinositol signaling system, were also represented in up- and down-regulated genes in TdBCK1. In the TdSLT2-69 mutant, the biosynthesis of other secondary metabolites was again the most represented pathway, whereas the other significantly represented KEGG pathways were similar to those in TdBCK1. When comparing the sectored progenies to those of the parental mutant strains, biosynthesis of other secondary metabolites, amino

acid metabolism, and carbohydrate metabolism pathways were significantly represented in TdBCK1-S1 (Fig. 7). However, the dominance of metabolic process pathways, such as biosynthesis of other secondary metabolites, amino acid metabolism, and carbohydrate metabolism, were diminished in TdSLT2-69-S1. For the 73 common DEGs, biosynthesis of other secondary metabolites was one of the two most represented pathways, with a total of 5 DEGs (Fig. 8). However,

Table 2. Functional study of common DEGs in comparisons between TdBCK1-S1 vs. TdBCK1 and TdSLT2-69-S1 vs. TdSLT2-69

JGI gene ID	Classification	Function description
338852	Metabolism	Polyketide synthase 4
258342	Transport	Putative sodium phosphate protein
85578*	Unknown	
356022*	Metabolism	Putative acid phosphatase
287230	Transport	Putative major facilitator superfamily transporter phosphate
358623	Metabolism	Putative Acetyl-coenzyme A carboxylase carboxyl transferase
245772	Transport	Putative potassium uptake protein
104198*	Structure	Cryparin
67838*	Unknown	
330996*	Signal transduction	S-adenosylmethionine-dependent methyltransferase-like protein
259317	Metabolism	Predicted protein
321522	Redox	Ferric reductase transmembrane
89535	Metabolism	Putative 3-phytase b precursor
355825*	Transport	Putative mfs peptide
348629*	Signal transduction	Phosphoesterase
273248	Transport	Putative low affinity copper transporter
109204*	Signal transduction	Putative zinc finger SWIM domain protein
358511*	protein-protein contact site	Kelch domain protein
356120*	protein-protein contact site	Kelch domain protein
357650*	protein-protein contact site	Kelch domain protein
322606*	protein-protein contact site	Kelch domain protein
358636*	protein-protein contact site	Kelch domain protein
346194	Signal transduction	Putative ankyrin repeat protein nuc-2
357023	Metabolism	Putative 5 3nucleotidase
355095	Unknown	Hypothetical protein UCRPA7_2558
248975*	Unknown	Putative gpi anchored
284134*	Redox	Putative ferric-chelate reductase
324303	Metabolism	Putative like family protein
280920	Metabolism	Putative fatty acid desaturase
320470	Structure	Putative cell wall protein
297116	Transport	H/K ATPase alpha subunit
322307	Metabolism	Putative perilipin mpl1-like protein
356370	Transport	Hypothetical protein CY34DRAFT_9264
58880	Structure	Zog-fe oxygenase
82322	Metabolism	Putative glycoside hydrolase family 16 protein
355877	Metabolism	Carboxypeptidase
346721	Metabolism	Putative dipeptidyl-peptidase 3
276559	Signal transduction	DCL2_CRYPA RecName
357263*	Signal transduction	Hypothetical protein V492_01086
255785	Signal transduction	Multiple ankyrin repeats single kh domain protein, putative
82840	Metabolism	IBR domain-containing protein
257472	Signal transduction	DEAD/DEAH box helicase
349858	Metabolism	Hypothetical protein SCLCIDRAFT_13763
287030*	Signal transduction	Putative wd g-beta repeat containing protein
256253	Structure	Putative von willebrand factor
233964	Metabolism	Hypothetical protein PFIC1_15243
270725	Signal transduction	Sir2 family protein
338832	Metabolism	FtsJ-like methyltransferase family protein
297135	Unknown	Hypothetical protein UCDDA912_g00277
267037	Structure	Heterokaryon incompatibility protein (het-6OR allele)
320080	Signal transduction	Putative rRNA-processing protein efg1
320079	Signal transduction	Putative zinc finger protein 251
70047	Structure	Hypothetical protein S40293_10774
356222	Structure	Putative tetraspanin tsp3
249345	Metabolism	Hypothetical protein S40285_08606
291140	Metabolism	Putative nad-dependent malic enzyme
345956	Metabolism	Putative aaa family
92416	Signal transduction	Hypothetical protein UCDDA912_g10323
287505	Metabolism	Adenine phosphoribosyltransferase
260943	Signal transduction	P-loop containing nucleoside triphosphate hydrolase protein
290551	Metabolism	Putative secreted aspartic proteinase protein
234408	Signal transduction	Putative ankyrin-like protein
356265*	Structure	Putative erythrocyte band 7 integral membrane protein
355167	Signal transduction	Putative cysteine and glycine-rich protein 3
225273*	Structure	Hypothetical protein CMQ_390
108074	Transport	Hypothetical protein UCRPA7_801
105038*	Metabolism	Putative catalase 1
324353*	Metabolism	Aspergillopepsin-2
342244*	Signal transduction	Putative aaa family
285834	Signal transduction	Putative BTB/POZ domain protein
342243	Signal transduction	Putative geranylgeranyl pyrophosphate synthetase protein
358242	Metabolism	Putative pepsin a1
336241	Transport	Putative calcium-translocating p-type ATPase

* indicates DEGs affected by the hypovirus infection

other metabolic KEGG pathways, such as amino acid metabolism, carbohydrate metabolism, and lipid metabolism pathways, were represented by only one or two DEGs. Interestingly, the MAPK signaling pathway was continuously represented with a single DEG, and the translation pathway was the most represented, with 5 DEGs. Considering that there were no DNA sequence changes in the sectorized progenies from their corresponding parental strains but that there were enormous inheritable phenotypic changes, the numerous DEGs in RNA metabolism, such as RNA degradation, mRNA surveillance, and RNA transport, suggested the existence of a genetic mechanism governing these inheritable phenotypic changes. A recent study revealed the global epigenetic changes accompanying sectorization (So et al., 2018). Thus, it would be interesting to examine the regulation of genes related to the biosynthesis of other secondary metabolites.

The 73 genes were further categorized by protein function (Table 2). In total, 24 genes were classified as genes involved in metabolic processes, and 19 were classified as genes involved in signal transduction, such as transcription factors or effectors. Nine genes were identified in both of structural proteins and transport, and two were involved in redox. Interestingly, five Kelch-domain containing isoforms were identified as overrepresented genes in the sectorized progenies. Five genes were identified as unknown functions. Therefore, genes related to transcription factors should be analyzed for their regulation and downstream effectors for inheritable sectorized phenotypes. Among these 73 DEGs, 22 DEGs which were affected by the hypovirus CHV1 infection are interesting (Table 2: * indicates DEGs affected by the hypovirus infection.). Hypoviral infection in *C. parasitica* resulted in characteristic phenotypic changes of hypovirulence and other associated symptoms such as reduced pigmentation and conidiation i.e., in general preventing appropriate

development of a host fungus and having the fungal host remain in juvenile stage without further differentiation (Dawe and Nuss, 2001). Moreover, other studies demonstrated the occurrence of sectoring morphology due to the mycovirus infections (Bhatti et al., 2011; Hammond et al., 2008; Wu et al., 2007). Therefore, these genes might represent the least number of hypoviral-specific sectorization effectors. The predicted function analysis of these hypoviral- and sectorization-specific genes suggested that five were classified as those related to genetic information processing such as helicase, DNA-binding protein, and DNA methyltransferase, which suggested the implication of specific regulatory mechanism for the process leading to sectorization. These results were in good agreement with recent study demonstrating global changes in DNA methylation in sectorized progenies (So et al., 2018). Interestingly, the cryparin gene, a highly expressed hydrophobin gene specifically down-regulated by hypovirus infection, was one of seven structural genes. A recent study revealed that cryparin expression was transcriptionally affected by three fungal representative MAPK signal transduction pathways (So and Kim, 2017). Our transcriptomic analysis showed down-regulation of cryparin in the CWI mutants such as TdBCK1 and TdSLT2-69 compared to the wild-type and up-regulation in the sectorized progenies compared to the corresponding parental strains, although cryparin expression was not recovered to the level of that in the wild-type, which was consistent with previous real time RT-PCR results (So and Kim, 2017). Considering the cellular location and biological function of cryparin (Kazmierczak et al., 2005; Kim et al., 2008), cryparin like other structural genes is highly unlikely to be the cause of sectorization; it is more likely the result of sectorization because it is necessary to support robust growth of mycelia. However, the regulatory hierarchy of cryparin expression helps to clarify the onset of the sectorization phenotype.

Table 3 Genes used for qRT-PCR analysis

JGI gene ID	Classification	Function description
356022	Metabolism	Putative acid phosphatase
104198	Structure	Cryparin
330996	Signal transduction	S-adenosylmethionine-dependent methyltransferase-like protein
355825	Transport	Putative mfs peptide
348629	Signal transduction	Phosphoesterase
358511	Protein-protein contact site	Kelch domain
284134	Redox	Putative ferric-chelate reductase
356265	Structure	Putative erythrocyte band 7 integral membrane protein
225273	Structure	Hypothetical protein
105038	Metabolism	Putative catalase
324353	Metabolism	Aspergillopepsin-2
342244	Signal transduction	Putative aaa family
287030	Unknown	Putative WD-40, G-beta repeat containing
357263	Unknown	Hypothetical protein
109204	Unknown	Unknown
248975	Unknown	Unknown
67838	Unknown	Unknown
85578	Unknown	Unknown

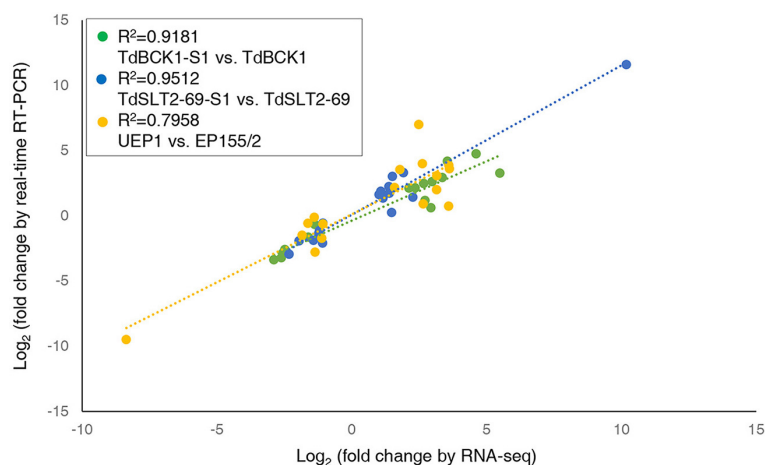


Fig. 9. The expression patterns of 18 genes were validated by RT-PCR. The X-axis represents \log_2 FC expression levels based on RNA-seq data. The Y-axis represents \log_2 FC expression levels based on real-time RT-PCR data. The data of linear regression analysis represented a significant correlation between the two platforms. R squared correlation values are indicated for each regression line.

Validation of DEGs by qRT-PCR analysis

To validate the DEGs, quantitative real-time RT-PCR (qRT-PCR) analysis was conducted on 18 candidate genes (Table 3), which represented all genes showing the significant fold changes caused by the presence of hypovirus as well as sectorization. Among these, 10 genes were upregulated and eight were downregulated in the presence of hypovirus. In addition, compared to the corresponding parental strains, 11 genes were upregulated and seven were downregulated in the sectorized progenies. The expression of each gene was calculated using the $2^{-\Delta\Delta CT}$ method, as previously described (Livak and Schmittgen, 2001). All selected genes showed expression levels in good agreement with those from the RNA-Seq analysis. Moreover, the linear regression analysis between two platforms of RNA-Seq and qRT-PCR indicated that the changes in the expression levels of target genes estimated by both platforms were highly correlated with R^2 values of 0.9181, 0.9512, and 0.7958 for comparisons between TdBCK1-S1 vs. TdBCK1, TdSLT2-69-S1 vs. TdSLT2-69, and UEP1 vs. EP155/2, respectively. Therefore, the qRT-PCR results validated the RNA-Seq analysis results (Fig. 9, Supplementary Table S2).

CONCLUSION

Genome-wide transcriptomic analysis of *Cryphonectria parasitica* mutants in components (i.e., orthologs of yeast *Bck1* and *Slt2*) of CWI-related MAPK pathways revealed a broad spectrum of metabolic changes accompanying the CWI MAPK pathway. Additionally, 70% of differentially expressed genes were common, and the remainder were specific to the components, suggesting that the orthologs of yeast *Bck1* and *Slt2* were in the same CWI MAPK pathway, although some component-specific genes existed. Then, sectorization-specific transcripts analysis between sectorized progenies and their corresponding parental mutant strains demonstrated that 73 genes were commonly affected between sectorized progenies and parental mutants. Moreover, according to gene ontology (GO) analysis, all 73 genes were enriched in secondary metabolism and translation. Function-

al analysis of the 73 genes indicated that many genes were implicated in signaling pathways, suggesting that several regulatory pathways are important in sectorization. Fungal sectorization, defined as robust growth without differentiation, occurs in many fungi. However, our understanding of the genetic mechanism underlying sectorization is limited. This study helps to clarify the genes of importance in sectorized progenies and the molecular consequences of fungal sectorization.

ACKNOWLEDGMENTS

This work was supported by the NRF grants by MSIP (2015R1A2A1A10055684 and 2018R1A2A1A05078682). Y-H. Ko were supported by BK21 PLUS program in the Department of Bioactive Material Sciences.

REFERENCES

- Allen, T.D., Dawe, A.L., and Nuss, D.L. (2003). Use of cDNA microarrays to monitor transcriptional responses of the chestnut blight fungus *Cryphonectria parasitica* to infection by virulence-attenuating hypoviruses. *Eukaryot. Cell* 2, 1253-1265.
- Anders, S., and Huber, W. (2010). Differential expression analysis of sequence count data. *Genome Biol.* 11, 106-10.1186/gb-2010-11-10-r106.
- Bhatti, M.F., Jamal, A., Petrou, M.A., Cairns, T.C., Bignell, E.M., and Coutts, R.H. (2011). The effects of dsRNA mycoviruses on growth and murine virulence of *Aspergillus fumigatus*. *Fungal Genet. Biol.* 48, 1071-1075.
- Bowman, S.M., and Free, S.J. (2006). The structure and synthesis of the fungal cell wall. *Bioessays* 28, 799-808.
- Chae, S., Kim, J.S., Jun, K.M., Lee, S.B., Kim, M.S., Nahm, B.H., and Kim, Y.K. (2017). Analysis of genes with alternatively spliced transcripts in the leaf, root, panicle and seed of rice using a long oligomer microarray and RNA-Seq. *Mol. Cells* 40, 714-730.
- Chen, B., Gao, S., Choi, G.H., and Nuss, D.L. (1996). Extensive alteration of fungal gene transcript accumulation and elevation of G-protein-regulated cAMP levels by a virulence-attenuating hypovirus. *Proc. Natl. Acad. Sci. USA* 93, 7996-8000.
- Choi, E.S., Chung, H.J., Kim, M.J., Park, S.M., Cha, B.J., Yang, M.S., and Kim, D.H. (2005). Characterization of the *ERK* homologue

- CpMK2 from the chestnut blight fungus *Cryphonectria parasitica*. *Microbiology* *1*, 1349-1358.
- Cox, M.P., Peterson, D.A., and Biggs, P.J. (2010). SolexaQA: at-a-glance quality assessment of Illumina second-generation sequencing data. *BMC Bioinform.* *11*, 1-6.
- Dawe, A.L., and Nuss, D.L. (2001). Hypoviruses and chestnut blight: exploiting viruses to understand and modulate fungal pathogenesis. *Annu. Rev. Genet.* *35*, 1-29.
- Deng, F., Allen, T.D., Hillman, B.I., and Nuss, D.L. (2007). Comparative analysis of alterations in host phenotype and transcript accumulation following hypovirus and mycoreovirus infections of the chestnut blight fungus *Cryphonectria parasitica*. *Eukaryot. Cell* *6*, 1286-1298.
- Hammond, T.M., Andrews, M.D., Roossinck, M.J., and Keller, N.P. (2008). *Aspergillus* mycoviruses are targets and suppressors of RNA silencing. *Eukaryot. Cell* *7*, 350-357.
- Kang, H.S., Choi, J.W., Park, S.M., Cha, B., Yang, M.S., and Kim, D.H. (2000). Ordered differential display from *Cryphonectria parasitica*. *Plant Pathol. J.* *16*, 142-146.
- Kazmierczak, P., Kim, D.H., Turina, M., and Van Alfen, N.K. (2005). A hydrophobin of the chestnut blight fungus, *Cryphonectria parasitica*, is required for stromal pustule eruption. *Eukaryot. Cell* *4*, 931-936.
- Kim, D.H., Rigling, D., Zhang, L., and Van Alfen, N.K. (1995). A new extracellular laccase of *Cryphonectria parasitica* is revealed by deletion of *LAC1*. *Mol. Plant-Microbe Interact.* *8*, 259-266.
- Kim, J.G., Lee, J.G., Kim, J.M., Park, J.A., Park, S.M., Yang, M.S., and Kim, D.H. (2010). A DnaJ-like homolog from *Cryphonectria parasitica* is not responsive to hypoviral infection but is important for fungal growth in both wild-type and hypovirulent strains. *Mol. Cells* *30*, 235-243.
- Kim, J.M., Kim, J.G., Yun, S.H., So, K.K., Ko, Y.H., Kim, Y.H., Park, S.M., and Kim, D.H. (2016). A mutant of the *Bck1* homolog from *Cryphonectria parasitica* resulted in sectorization with an impaired pathogenicity. *Mol. Plant-Microbe Interact.* *29*, 268-276.
- Kim, M.J., Kwon, B.R., Park, S.M., Dhung, H.J., Yang, M.S., Churchill, A.C.L., Van Alfen, N.K., and Kim, D.H. (2008). Promoter analysis of the cell surface-abundant and hypoviral-regulated cryparin gene from *Cryphonectria parasitica*. *Mol. Cells* *26*, 496-502.
- Langmead, B., Trapnell, C., Pop, M., and Salzberg, S.L. (2009). Ultrafast and memory-efficient alignment of short DNA sequences to the human genome. *Genome Biol.* *10*, 25-34.
- Li, A., Begin, M., Kokurewicz, K., Bowden, C., and Horgen, P.A. (1994). Inheritance of strain instability (sectoring) in the commercial button mushroom, *Agaricus bisporus*. *Appl. Environ. Microbiol.* *60*, 2384-2388.
- Li, B., Routti, V., Stewart, R.M., Thomson, J.A., and Dewey, C.N. (2010). RNA-seq gene expression estimation with read mapping uncertainty. *Bioinformatics* *26*, 493-500.
- Livak, K.J., and Schmittgen, T.D. (2001). Analysis of relative gene expression data using real-time quantitative PCR and the $2^{-\Delta\Delta CT}$ method. *Methods* *25*, 402-408.
- Magae, Y., Akahane, K., Nakamura, K., and Tsunoda, S. (2005). Simple colorimetric method for detecting degenerate strains of the cultivated basidiomycete *Flammulina velutipes* (Enokitake). *Appl. Environ. Microbiol.* *71*, 6388-6389.
- Moon, K.B., Ahn, D.J., Park, J.S., Jung, W.Y., Cho, H.S., Kim, H.R., Jeon, J.H., Park, Y.I., and Kim, H.S. (2018). Transcriptome profiling and characterization of drought-tolerant potato plant (*Solanum tuberosum* L.). *Mol. Cells* *41*, 979-992.
- Park, J.A., Kim, J.M., Park, S.M., and Kim, D.H. (2012). Characterization of *CpSte11*, a MAPKKK gene *Cryphonectria parasitica*, and initial evidence of its involvement in the pheromone response pathway. *Mol. Plant Pathol.* *13*, 240-250.
- Park, S.M., Choi, E.S., Kim, M.J., Cha, B.J., Yang, M.S., and Kim, D.H. (2004). Characterization of HOG1 homologue, CpMK1, from *Cryphonectria parasitica* and evidence for hypovirus-mediated perturbation of its phosphorylation in response to hypertonic stress. *Mol. Microbiol.* *51*, 1267-1277.
- Ryan, M.J., Bridge, P.D., Smith, D., and Jeffries, P. (2002). Phenotypic degeneration occurs during sector formation in *Metarhizium anisopliae*. *J. Appl. Microbiol.* *93*, 163-168.
- Sheng, T.C. (1951). The genetic basis of woolly degeneration in *Neurospora crassa*. *Bot. Gaz.* *113*, 203-206.
- So, K.K., and Kim, D.H. (2017). Role of MAPK signaling pathways in regulating the hydrophobin cryparin in the chestnut blight fungus *Cryphonectria parasitica*. *J. Mycolobiol.* *45*, 362-369.
- So, K.K., Ko, Y.H., Chun, J., Bal, J., Jeon, J., Kim, J.M., Choi, J., Lee, Y.H., Huh, J.H., and Kim, D.H. (2018). A global DNA methylation in *Cryphonectria parasitica* and genome-wide changes in DNA methylation of a sectorized progeny of *CpBck1* mutant. *Front. Plant Sci.* *9*, 103.
- So, K.K., Ko, Y.H., Chun, J., Kim, J.M., and Kim, D.H. (2017). Mutation of the *Slt2* ortholog from *Cryphonectria parasitica* results in abnormal cell wall integrity and sectorization with impaired pathogenicity. *Sci. Rep.* *7*, 9038.
- Sun, Q., Choi, G.H., and Nuss, D.L. (2009). Hypovirus-responsive transcription factor gene *pro1* of the chestnut blight fungus *Cryphonectria parasitica* is required for female fertility, asexual spore development, and stable maintenance of hypovirus infection. *Eukaryot. Cell* *8*, 262-270.
- Turina, M., Zhang, L., and Van Alfen, N.K. (2006). Effect of *Cryphonectria hypovirus 1* (CHV1) infection on Cpkk1, a mitogen-activated protein kinase of the filamentous fungus *Cryphonectria parasitica*. *Fungal Genet. Biol.* *43*, 764-774.
- Wang, C.S., Skrobek, A., and Butt, T.M. (2004). Investigations on the destruxin production of the entomopathogenic fungus *Metarhizium anisopliae*. *J. Invertebr. Pathol.* *85*, 168-174.
- Wu, M.D., Zhang, L., Li, G.Q., Jiang, D.H., Hou, M.S., and Huang, H.C. (2007). Hypovirulence and double-stranded RNA in *Botrytis cinerea*. *Phytopathology* *97*, 1590-1599.